Sources of Inaccuracy in Boron Isotope Measurement Using LA-MC-ICP-MS

Jan **Fietzke*** (iD) and Eleni **Anagnostou**

GEOMAR Helmholtz Center for Ocean Research Kiel, Wischhofstrasse 1–3, 24118 Kiel, Germany
* Corresponding author. e-mail: jfietzke@geomar.de

Laser ablation multi-collector-inductively coupled plasma-mass spectrometry (LA-MC-ICP-MS) has become a valuable tool for the *in situ* measurement of the boron isotope composition of geological samples at high (tens to hundreds of μm) spatial resolution. That said, this application suffers from significant analytical challenges. We focus in this study on the underlying processes of two of the main causes for inaccuracies using this technique. We provide empirical evidence that not only Ca ions (Sadekov *et al.* 2019, Standish *et al.* 2019, Evans *et al.* 2021) but also Ar ions, that are reflected within the flight tube of the mass spectrometer, are the source for previously reported issues with spectral baselines. We also address the impact of plasma conditions on the instrumental mass fractionation as a source for matrix- and mass-load-related analytical biases. Comparing experimental data with the results of a dedicated release and diffusion model (RDM) we estimate that a close to complete ($\sim$ 97%) release of boron from the sample aerosol is needed to allow for consistently accurate LA boron isotope measurement results without the need for corrections.

Keywords: boron isotopes, laser ablation, scattered ions, mass fractionation, plasma conditions.

Boron is one of the lightest and least abundant elements in the periodic table. It consists of two isotopes (^{10}B and ^{11}B) with the heavier one being about four times more abundant. Boron's physio-chemical characteristics result in one of the largest ranges of naturally occurring mass-dependent isotope fractionation ($\sim$ 100‰) in nature (Marschall and Foster 2018). Applications of boron isotope fractionation in natural reservoirs have been developed in both, high- and low-temperature geochemistry, as well as cosmochemistry (Palmer and Swihart 1996). In recent years boron isotopes have been of particular interest for marine isotope geochemists focusing on marine biogenic carbonates to study the marine carbon pool and its link to atmospheric CO_2.

Per convention, boric acid NIST SRM 951 has been adopted as the certified isotopic reference material (Catanzaro *et al.* 1970, May and Gills 1999). Boron isotope data of natural samples are commonly reported (as permil deviation) relative to the NIST SRM 951 reference value using the δ-notation:

$$\delta^{11}B = \left(\left(^{11}B/^{10}B\right)_{sample} / \left(^{11}B/^{10}B\right)_{NIST\ SRM\ 951} \right) - 1 \quad (1)$$

A variety of analytical methods has been developed for the measurement of boron isotopes, most prominently the bulk techniques thermal ionisation mass spectrometry (TIMS) (e.g., McMullen *et al.* 1961, Spivak and Edmond 1986, Hemming and Hanson 1992, Foster *et al.* 2006) and multi-collector inductively coupled plasma-mass spectrometry (MC-ICP-MS) (e.g., Lecuyer *et al.* 2002, Aggarwal *et al.* 2003, Foster 2008), and the *in situ* technique with secondary ion mass spectrometry (SIMS) (e.g., Chaussidon *et al.* 1997). More recently, laser ablation multi-collector inductively coupled plasma-mass spectrometry (LA-MC-ICP-MS) has been added to the *in situ* boron isotope technique (e.g., Le Roux *et al.* 2004). Based on the boron amount utilised per analysis, the choice of analytical technique allows for optimising either for precision (bulk techniques) or spatial resolution (*in situ* techniques), two occasionally conflicting goals which need to be carefully considered based on the specific scientific question and sample material. For example, there are orders of magnitude

differences in B mass fraction between tourmaline (% m/m of boron) and marine carbonates (μg g^{-1} mass fraction of boron). The analytical capabilities place LA-MC-ICP-MS somewhere in between the conventional bulk and *in situ* techniques. Being usually less precise than bulk techniques (due to lower total B amount utilised and absence of B preconcentration and matrix separation) it can achieve comparable spatial resolution to SIMS. Major benefits of LA-MC-ICP-MS are its versatility, speed and lack of elaborate sample pretreatment (i.e., boron separation from the sample matrix), which also strongly reduces blank and column related fractionation issues (Foster *et al.* 2018 and references therein). These benefits offered an opportunity to apply LA-MC-ICP-MS as an imaging tool for the B distribution in heterogeneous samples (Fietzke *et al.* 2015, Chalk *et al.* 2021, Fietzke and Wall 2022). Major disadvantages of LA-MC-ICP-MS applied for *in situ* B isotope measurements remain limitations in precision and challenges in proving accuracy of the analyses in particular when considering differences in the sample main matrix and the B mass fraction.

Considerable efforts have been made to improve the accuracy and precision of boron isotope measurements (e.g., Gonfiantini *et al.* 2003, Aggarwal *et al.* 2009). For bulk techniques this effort (i.e., performing round-robin studies) has resulted in good consistency of boron isotope data from different laboratories using different analytical techniques with focus on materials consisting of calcium carbonate (Gutjahr *et al.* 2021).

Since such effort has not been accomplished for boron isotope measurements with LA-MC-ICP-MS the current practice is the use of reference materials (RMs) that have been well characterised by bulk-solution techniques. This has resulted in the use of a range of commonly available RMs, both non-matrix matched (soda-lime glasses NIST SRM 610/612) and matrix-matched RMs (carbonate pressed-powder pellets of GSJ's *Porites sp.* coral JCp-1 and *Tridacna gigas* JCt-1, USGS MACS-3, UWC-1) as well as in-house carbonate RMs (inorganic calcite eBlue, calcitic octocoral PS69/318-1, aragonite WP 22) (e.g., Le Roux *et al.* 2004, Fietzke *et al.* 2010, Sadekov *et al.* 2019, Standish *et al.* 2019, Evans *et al.* 2021, Chalk *et al.* 2021, Raitzsch *et al.* 2020, Babila *et al.* 2022).

More recently, systematic biases in δ^{11}B determination using LA-MC-ICP-MS have been demonstrated (Sadekov *et al.* 2019, Standish *et al.* 2019, Evans *et al.* 2021). These studies report offsets of up to ~ 20‰ towards lighter apparent boron isotope ratios which are closely related to the B/Ca concentration ratio of the sample/RM and to a change in the spectral baseline around the ^{10}B peak. These observations were attributed to scattered ions of Ca, C or O, potentially changing the spectral baseline, and as such empirical correction schemes were proposed (Sadekov *et al.* 2019, Standish *et al.* 2019, Evans *et al.* 2021). Notably, all three mentioned studies used a similar type of MC-ICP-MS (Thermo Neptune Plus). In contrast, analytical offsets of comparable degree have not been reported in studies using other MC-ICP-MS types i.e., the AXIOM (Thermo Scientific) or the Plasma II (Nu Instruments) (Fietzke *et al.* 2010, Wall *et al.* 2019, Mayk *et al.* 2020, Raitzsch *et al.* 2020, Fietzke and Wall 2022). It is an open question, if or to what extent the analytical biases/background responses are instrument-specific or if other details are contributing as well, such as e.g., the use of ion-counters *vs.* Faraday cups, mass load, plasma conditions, type of laser used (Mayk *et al.* 2020, Fietzke and Wall 2022).

To further investigate the sources of the analytical biases in boron isotope measurement using LA-MC-ICP-MS, we attempt to conceptualise the problem and its complexity (Figure S1) and we differentiate between general features (e.g., impact of plasma conditions) and instrument-specific effects.

We focus on observable changes of the spectral background (mostly around the ^{10}B mass peak) and a comparison of different types of MC-ICP-MS. Since earlier studies have already pointed towards scattered Ca ions as a potential source of the reported analytical biases, we prepared a Ca-free B in-house RM which we use for tests and during routine analyses. Besides the background-related issues we focus more broadly on the instrumental mass fractionation involved in measuring B isotope ratios using LA-MC-ICP-MS. We investigate the impact of plasma conditions and propose a model that is based on the gradual release and diffusion of boron in the plasma to explain the observed trends in boron isotope data for different matrix materials.

Experimental

We used three typical MC-ICP-MS instruments to allow the identification of which analytical problems are instrument-specific and to further interrogate remaining issues.

The MC-ICP-MS instruments used were the AXIOM (ThermoScientific; originally designed and manufactured by VG), the Neptune Plus and the Nu Instruments Plasma3. The laser ablation systems utilised were the NWR UP193fx (in

combination with AXIOM) and the Teledyne Cetac Analyte Excite (in combination with the Neptune Plus and Nu Plasma3).

Both LA systems have 193 nm ArF excimer laser sources from ATL with similar energy and pulse duration characteristics. Additionally, both systems were equipped with two-volume ablation cells providing very similar wash-out times. To further allow for direct comparison of results from the two laser systems, they were operated using comparable gas flow rates of He, energy densities, spot sizes and repetition rates and therefore no analytical offsets because of LA system used are expected.

We performed a series of systematic tests using different plasma conditions while keeping the conditions for the LA system constant (constant He cell gas flow, constant laser fluence, spot size and repetition rate). Broadly, instrumental parameters were 1000–1200 W for the rf power, 17 l min^{-1} Ar cool gas, $\sim$ 0.8 l min^{-1} Ar auxiliary gas, 0.7–1.0 l min^{-1} Ar sample gas and 0.7–1.0 l min^{-1} He ablation cell gas. Typical operating parameters can be found in Table S1. Changes in the plasma condition have been evaluated using the NAI metric (Fietzke and Frische 2016). The normalised argon index (NAI) is defined as NAI = 2*^{38}Ar/^{40}Ar$_2$ and quantifies the balance between Ar ionisation and Ar$_2$ cluster ion formation, i.e., a higher NAI represents hotter plasma conditions. Plasma conditions were adjusted by varying only rf power and sample gas flow (Ar added downstream to the He gas exiting the ablation cell). After each change of the former parameters the plasma was allowed time to stabilise (minimum 30 min) before the ion optics were tuned for maximum signal intensity and optimal peak shape using the ^{12}C mass peak of the gas blank. ^{12}C is a convenient isotope for ion optics tuning, since its mass is close to the boron isotope masses and it is usually present at sufficiently high and stable signal intensity in the gas blank.

Results and discussion

The systematics of changing baselines in response to argon and calcium ions

Recently published studies provided evidence that variable baselines collected on Faraday cups can be a main source of inaccuracies in LA-MC-ICP-MS determination of boron isotopes (Sadekov *et al.* 2019, Standish *et al.* 2019, Evans *et al.* 2021). Using a similar type of MC-ICP-MS (Thermo Neptune Plus) they have consistently shown a baseline signal which mostly impacts the spectral

region around the ^{10}B mass peak and is characterised by a pronounced baseline intensity maximum at the low mass side of the ^{40}Ar^{4+} and ^{10}B$^+$ mass peaks. Additionally, these studies revealed that this baseline is responding to the introduction of ablated material attributing this to scattered Ca ions.

Based on our previous work on the impact of plasma conditions on the analytical performance of ICP-MS (Fietzke and Frische 2016) we carried out tests using a Thermo Neptune Plus. The aim was to investigate the impact of changing plasma conditions on the spectral baseline. The collector set-up was as follows: L4 collecting ^{10}B aligned with H3 collecting ^{11}B for a centre mass of $\sim$ 10.505 amu, both using 10^{12} ohm amplifiers. Simultaneously, IC6 (CDD – compact discrete dynode ion counter) collects the ion intensities at $\sim$ 0.1 amu below L4.

Two separate test series were performed using 1000 W and 1200 W rf power. The plasma conditions were modified in both tests by changing the Ar sample gas flow admixed to the constant He ablation cell gas flow coming from the LA unit. ^{38}Ar and ^{40}Ar$_2$ (80 amu) were measured for each plasma condition to calculate the normalised Ar index NAI (Fietzke and Frische 2016).

In Figure 1 the baseline scans (gas blank) around the ^{10}B mass peak for six different plasma conditions (NAI 0.3–6.7) using 1200 W rf power are displayed. While the pattern of the baseline signal appears robust, it reveals a systematic increase related to ^{38}Ar intensities measured for each plasma condition. No significant differences in the pattern of the baseline and the response on ^{38}Ar were observed in the test series using 1000 W rf power (see Figure S2).

During the B isotope multi-collection analysis (L4: ^{10}B and H3: ^{11}B) the magnet was centred at 10.505 amu, simultaneously collecting the IC6 baseline intensity. Comparing those intensities with the respective baseline maximum intensities (at $\sim$ 10.54 amu) shows a tight correlation between the two, independent of whether the test was performed at 1000 W or 1200 W (Figure S3). This indicates that the general response of the baseline can be represented equally well by either of the two spectral positions (10.54 amu or 10.505 amu), i.e., data collected at 10.505 amu are a fair representation of baseline changes.

The systematic increase in baseline intensities (Figure 1) is not caused directly by the NAI, but by the Ar ion intensity, which results from the plasma condition, interface transmission and ion optics tuning. The highest NAI tested
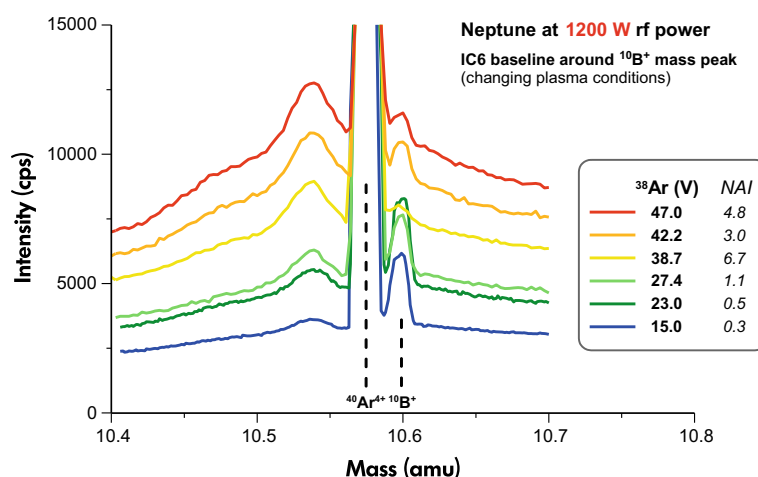
Figure 1. Spectral baseline scans (gas blank) measured on IC6 under different plasma condition. The ^{10}B intensity in the gas blank changes systematically with NAI because of the differences in B sensitivity (see also supplement's Figure S4), decreasing with increasing NAI.

(NAI = 6.7) resulted in a lower ^{38}Ar intensity and consequently lower baseline intensity than the two lower NAIs of 3 and 4.8.
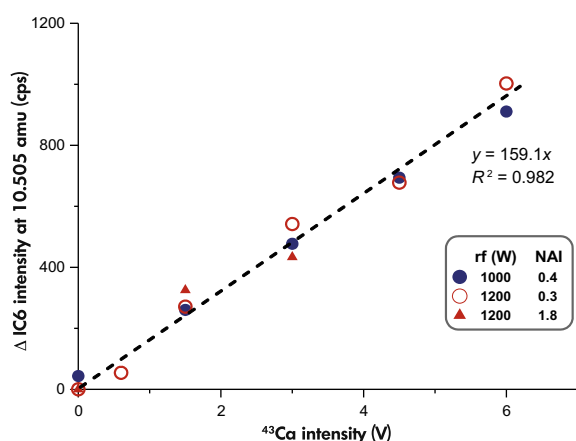
The relationship between the baseline intensity measured at 10.505 amu and the ^{38}Ar intensity measured for the respective plasma condition is shown in Figure 2. The baseline intensities measured during both (1000 W and 1200 W) test series scale on a common trend with the ^{38}Ar intensity measured for the respective plasma condition.
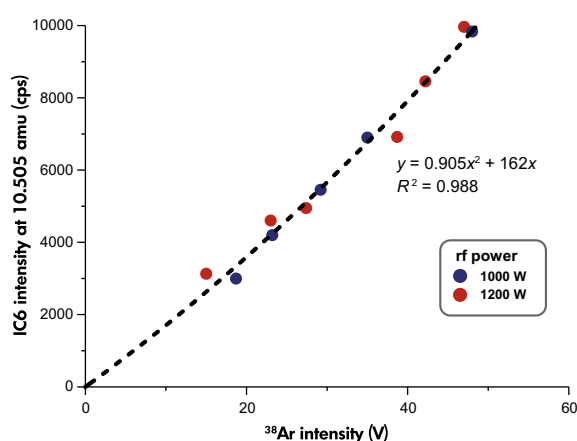
Figure 2. ^{38}Ar intensity and corresponding baseline intensity measured at 10.505 amu (IC6) from both test series (1000 W and 1200 W rf). Each data point represents different plasma conditions and accordingly tuned ion optics. The fit is based on all displayed data.

For a number of different plasma conditions, after tuning for optimal ion optics settings, we measured the response (change) of the IC6 baseline to the introduction of ablated material. For this test a coralline alga sample was used and ablated at different laser repetition rates to modify the material supply to the plasma. The ^{43}Ca intensity was measured under each test condition prior to the baseline response data acquisition (Figure 3). While starting at different gas blank baseline intensities ($\sim$ 3500 cps for the lower NAI and $\sim$ 6500 cps for the higher NAI) the change in the 10.505 amu baseline intensity followed a common linear trend in response to the respective ^{43}Ca intensity measured.

We observed distinct linear responses of the spectral baseline to both ^{38}Ar and ^{43}Ca, representing argon and calcium ion intensities. The fact that both elements have one isotope of similar mass in common (40 amu), which additionally is the isotope of highest abundance of each respective element, in our opinion suggests that ^{40}Ar and ^{40}Ca are the main sources of the observed baseline. A likely mechanism would be the reflection of those ions' beam at the high mass side of the flight tube as already proposed in previous studies (Sadekov *et al.* 2019, Standish *et al.* 2019, Evans *et al.* 2021). This would explain the observed responses and the shape of the baseline, the latter not representing a focused but rather a broad, unfocussed ion beam. The proposed mechanism is further supported by the comparable baseline response on the approximated primary intensity of the respective isotope at 40 amu. Converting both ^{38}Ar and ^{43}Ca intensities measured into the corresponding ^{40}Ar and ^{40}Ca intensities using the natural

© 2023 The Authors. *Geostandards and Geoanalytical Research* **published by John Wiley & Sons Ltd on behalf of the International Association of Geoanalysts.**

Figure 3. Change in baseline intensity (10.505 amu, IC6) in response to ^{43}Ca introduced by ablation of a carbonate sample (coralline alga). The linear fit is based on all displayed data.

isotope abundances of argon and calcium (not including isotope mass fractionation) results in baseline contributions of 0.14 cps V^{-1} of ^{40}Ar and 0.22 cps V^{-1} of ^{40}Ca which are of similar order of magnitude. We suspect the slightly higher sensitivity in the ^{40}Ca case points towards a higher probability of calcium ions to maintain their charge in the reflection on the flight tube surface due to its lower first ionisation potential when compared with argon (IP$_{Ca}$ = 6.11 eV vs. IP$_{Ar}$ = 15.76 eV).

Before correcting for the effect of such baseline changes on the measured B isotope data we test another aspect: How well does the baseline measured on the IC track the baseline intensities on the Faraday cups used for the actual boron isotope data acquisition? As above, we used baseline scan data obtained under different plasma conditions, and we compared the baseline data for ^{10}B (L4) and ^{11}B (H3) interpolated (to 10.505 amu) from the off-peak intensities (low: 10.45 amu and high mass side: 10.55 amu) with the IC6 intensity measured at 10.505 amu (Figure 4).

Two observations stand out: First, the baseline scans of both Faraday cups are correlated linearly to the baseline measured by the ion counter IC6, despite the fact that the test series covered a range of different plasma condition for two distinct rf power settings. This indicates IC6 can indeed be used to track the Faraday cup baseline changes. Second, there is the approximately three times stronger impact of baseline changes on the L4 (used for ^{10}B) compared with H3 (used for ^{11}B). Combining this estimate with the typical measured abundance ratio of boron isotopes ($^{11}B/^{10}B \sim 4.6–4.8$) results in an approximately fourteen-

fold stronger relative sensitivity of the ^{10}B compared with ^{11}B to baseline changes.

These observations are in overall agreement with the baseline characteristics reported in previous studies using a similar type of MC-ICP-MS (Thermo Neptune Plus) (Sadekov et al. 2019, Standish et al. 2019, Evans et al. 2021). Therefore, we consider this behaviour to be a common feature of the particular instrument and most likely caused by the specific design of the flight tube geometry.

This leaves us with the question how other types of MC-ICP-MS compare in this regard. We therefore tested the respective baseline behaviour for AXIOM and Nu Plasma 3 instruments in a similar way to the Thermo Neptune Plus. Examples of baseline scans can be found in Figure S5. All three types of MC-ICP-MS display an increase in scattered-ion background intensity around the mass peak of ^{10}B. This is suppressed typically by about three orders of magnitude for all three instruments if the ions are measured not on Faraday cups (or in case of Neptune Plus CDD ion counters, too) but by ion counters after beam deflection. This supports previous observations using the ion counter (with RPQ - retarding potential quadrupole) on a Neptune Plus (Standish et al. 2019). Our data indicate that for all three types of MC-ICP-MS tested in this study, the baseline and its potential changes need to be monitored and corrected for when boron isotopes are measured via laser ablation using Faraday cups (or ion counters without beam deflectors).

More specifically, the baseline itself is not the main problem, instead it is the baseline change in response to the introduction of material and the corresponding Ca ions. Additionally, the balance between B signal intensity and baseline intensity change defines the analytical offset from scattered ion background. We have measured the baseline responses in relation to the ^{43}Ca ion signal intensity (measured ablating carbonate) for each of the three MC-ICP-MS. The changes in baseline voltages per volt of ^{43}Ca measured for both ^{10}B and ^{11}B using each of the three instruments (in different detector configurations) are summarised in Table 1. We use these data to calculate the expected effect (apparent shift in boron isotope ratio $\Delta\delta^{11}B$) for two examples of $^{11}B/^{43}Ca$ signal intensity ratios (0.01 and 0.03) for illustration (see Table 1).

The contributions of scattered ions to the baselines of ^{10}B and ^{11}B for the different types of MC-ICP-MS are mostly depending on the respective detectors used. The strongest baseline suppression can be observed ion counters in combination with beam deflection, which are positioned behind the focal plane of the Faraday cups. This further
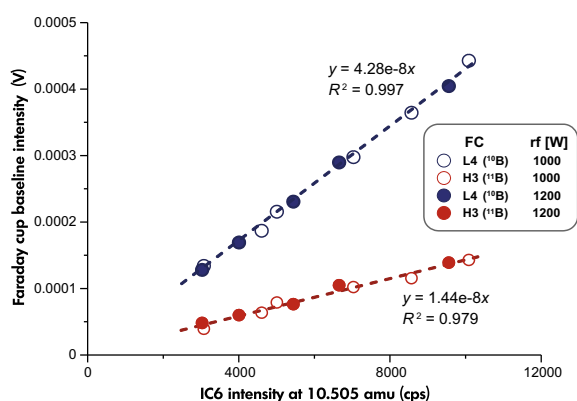
Figure 4. Interpolated Faraday cup baselines for ^{10}B and ^{11}B in response to intensity measured at IC6.

supports that the source of the baseline change is ions scattered inside of the flight tube. Such ions enter the collector array at a different angle and seem to be effectively separated from the focused beams of boron ions by beam deflectors.

Instrumental boron isotope mass fractionation I: The interplay of plasma condition and sample matrix

If the correction for (changing) contributions of scattered Ar and Ca ions would suffice to obtain accurate B isotope data via LA-MC-ICP-MS, no matrix-dependent offsets should be observed. This is unfortunately not the case (e.g., Evans et al. 2021, Figure 5 therein), resulting in distinct correction trends in B isotope offsets for silicate glass and carbonate reference materials measured relative to NIST SRM 612. Furthermore, the mass-load effect shown in figure S1 of Sadekov et al. (2019) cannot be explained by the impact of scattered ions alone. Since the B/Ca ratio is impacted only to a small degree by mass-load changes (i.e., changing laser spot size and repetition rate), the trend of lighter apparent boron isotope ratios with increasing mass-load cannot be fully accounted for through a baseline correction approach.

We suspect that one of the main causes of matrix-dependent offsets is the differing behaviour of the respective sample matrices within the ICP plasma, namely the specific degree of atomisation/ionisation and mass fractionation by radial diffusion. The logic behind this is, the earlier a sample atom/ion is released the more it is impacted by diffusion, resulting in a larger relative depletion of the lighter ions in the core of the plasma and consequentially where the ions are sampled.

To conceptualise the matrix/mass load-dependent fractionation effects we rely on two additional sets of experimental data. The first is based on analyses of reference materials (JCp-1, NIST SRM 610 and epo-951) collected over several sessions and at different NAIs over the last ~ 5 years (Figure 5). Details on the preparation and chemical characterisation of epo-951 in-house RM material are provided in the supplements. In brief, this calcium-free epoxy-based pellet carries the B isotope signature of NIST SRM 951 at a B/C concentration ratio of ~ 450 µmol mol^{-1} (for comparison: C/Ca molar ratio of ~ 1 in carbonates). Both JCp-1 and NIST SRM 610 data were normalised to epo-951. All data were acquired using the AXIOM in multi-ion-counting mode, which is not sensitive to the scattered ion effect because of the deflector's suppression of scattered ions when ion counters are used.

As can be seen in Figure 5 for high NAI (hot plasma conditions) the δ^{11}B composition of the RMs agree with the published values of δ^{11}B = 0 ± 0.3‰ (NIST SRM 610, Jochum et al. 2011) and δ^{11}B = 24.36 ± 0.45‰ (JCp-1, Gutjahr et al. 2021).

Towards low NAI (cool plasma conditions), the RMs gradually shift from their expected values. NIST SRM 610 is shifted towards heavier and JCp-1 towards lighter apparent δ^{11}B values. The matrix-specific offsets become negligible above NAI of ~ 4–5. The downside of the matrix tolerance achieved for hotter plasma conditions is a significant loss in signal intensity. Typical sensitivity vs. NAI behaviour can be found in Figure S4.

It needs to be highlighted that when using multi-ion-counting (Figure 5) we strictly limited the maximum ^{11}B intensity to 100 kcps, thus maintaining the mass load at relatively low levels. This avoids issues with detector linearity and dead time characteristics, but then the features shown in Figure 5 may shift for high mass load, presumably towards higher NAI, i.e., the point of negligible matrix-dependency is reached at hotter plasma conditions. In our opinion the trend towards lighter apparent B isotope ratios with increasing mass-load (Sadekov et al. 2019) implies an increase in the offsets shown in Figure 5 at low NAI and a shift of the intercept of measured and expected δ^{11}B values towards higher NAI for higher mass loads. Therefore, our NAI estimate of 4–5 for negligible matrix-specific offsets, which is obtained in a low mass-load experiment, most likely represents a lower limit.

A second set of experimental data has been collected in a dedicated NAI vs. fractionation experiment using the epo-951, a carbon-based material (see supporting information

Table 1.

Changes in off-peak baseline intensities for ^{10}B and ^{11}B in response to ^{43}Ca signal intensity for different types of MC-ICP-MS using different detector configurations (FC: Faraday cup, CDD: compact discrete dynode ion counter attached to Faraday cups, ICs: ion counters including beam deflection, positioned behind focal plane of Faraday cups, RPQ: retarding potential quadrupole). Resulting changes in measured $\delta^{11}B$ values for $^{11}B/^{43}Ca$ intensity ratios of 0.01 and 0.003, respectively, using a $^{11}B/^{10}B$ intensity ratio of 4.7 for the calculation

| MC-ICP-MS instrument	Detectors	$\Delta^{10}B_{baseline}/^{43}Ca$ (V/V)	$\Delta^{11}B_{baseline}/^{43}Ca$ (V/V)	$\Delta\delta^{11}B$ at $^{11}B/^{43}Ca$ = 0.01 (‰)	$\Delta\delta^{11}B$ at $^{11}B/^{43}Ca$ = 0.003 (‰)
Neptune Plus	FCs and CDDs	6.8e-6	2.3e-6	-3.0	-9.8
	ICs (defl./RPQ)	2.0e-9	0.5e-9	-0.001	-0.003
Axiom	FCs	5.9e-6	7.1e-6	-2.1	-6.8
	ICs (defl.)	5.8e-9	8.1e-8	0.005	0.018
NuPlasma3	FCs	4.5e-6	2.3e-6	-1.9	-6.2
	ICs (defl.)	3.3e-9	7.2e-9	-0.001	-0.003

for material description). Since epo-951 does not contain significant amounts of Ca it is not impacted by the scattered ion effect discussed before. Therefore, those experiments were performed using Faraday cups on both the AXIOM and the Neptune-plus (Figure 6).

The results reveal (a) large (~ 130–190‰) instrumental B isotope fractionation depending on the plasma condition and (b) systematic trends in fractionation vs. NAI. At low NAI (cold plasma conditions) we observe the lowest degree of instrumental fractionation, but the highest rate of change in fractionation with changing NAI. The fractionation stabilises for hot plasma conditions (high NAI) at its respective maximum. We additionally observe a significant offset

between the fractionation curves depending on the cone condition (on the AXIOM MC-ICP-MS), trending higher for clean/open skimmer cone compared with data collected with a heavily coated skimmer cone. We interpret this as an indication that instrumental mass fractionation is dominated by (at least) two major sources: (a) fractionation within the plasma, being dependent on the plasma condition and (b) fractionation within the interface, being dependent on cone conditions. The later can be caused by a combination of sources such as interface geometry (including cone geometry and distance) and interface pressure.

Comparing the Neptune plus with the AXIOM data confirms the fractionation sensitivity at low NAI. Notably, the
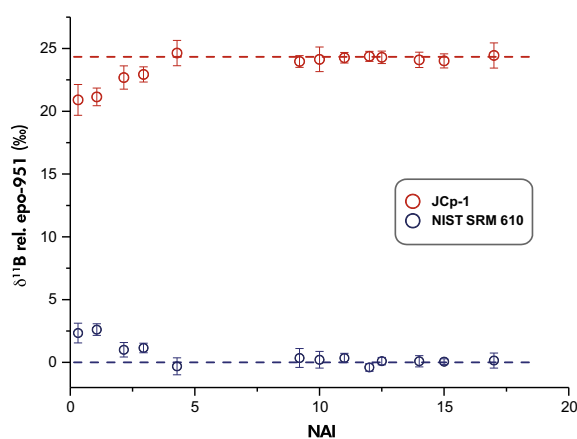
Figure 5. $\delta^{11}B$ results for reference materials JCp-1 (carbonate) and NIST SRM 610 (soda-lime glass) measured relative to epo-951 under different plasma conditions (NAI). Dashed lines represent $\delta^{11}B$ = 0‰ (blue; NIST SRM 610 from Jochum *et al.* 2011) and $\delta^{11}B$ = 24.36‰ (red; JCp-1 from Gutjahr *et al.* 2021).
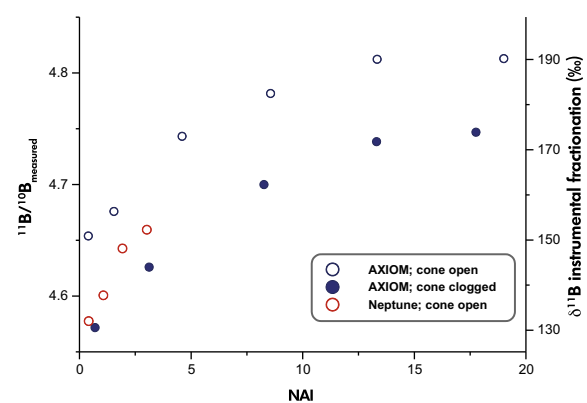
Figure 6. Measured $^{11}B/^{10}B$ ratio of epo-951 for different plasma conditions (NAI). For context the right-hand *y*-axis provides the $\delta^{11}B$ equivalent of the instrumental fractionation relative to the certified NIST SRM 951 boron isotope ratio of $^{10}B/^{11}B$ of 0.2473 (May and Gills 1999).
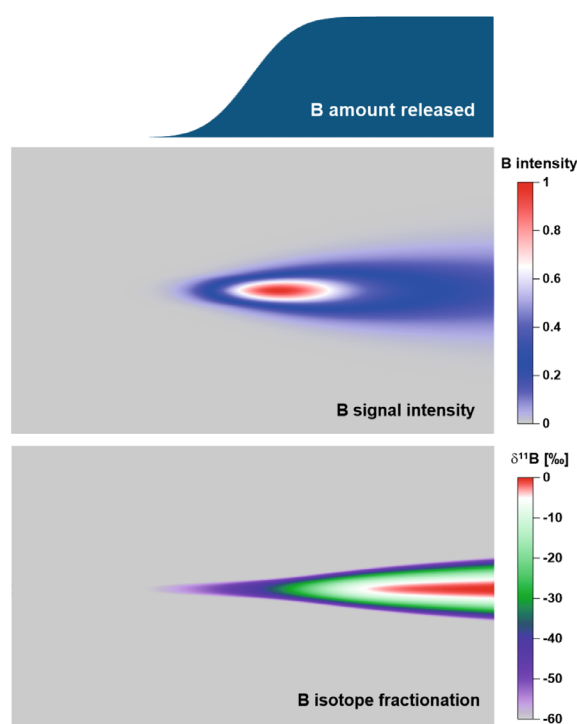
Figure 7. Results of one example run of the release and diffusion model (RDM). In the model the sample aerosol is injected from the left side, B is gradually released at the centre axis and undergoes mass-dependent fractionation for both, ^{10}B and ^{11}B. Both, B intensity and B isotope fractionation are normalised to their respective maximum values. For more examples see supporting information.

experiment for the Neptune-plus had been limited to the lower end of the NAI range of interest. The ion optics of the Neptune-plus do not allow for a satisfying focus of the ion beam at higher NAI.

When evaluating the AXIOM results and normalising each of both experiments' trends to the respective stable value at high-NAI, we obtain a common trend in B isotope fractionation vs. NAI, regardless of the cone and interface condition (see supporting information). Using this trend, we estimate a mean B instrumental mass fractionation of ~ -35‰ at NAI of 0.6 (maximum B signal intensity; see Figure S4 and supporting information). Additionally, we use this trend to estimate the degree of B instrumental mass fractionation at NAI of 4-5, our estimated limit in plasma condition for minimising matrix-dependent offsets (Figure 5), to be ~ -17.5‰. Above NAI of 4-5, all three tested materials respond in a similar way with respect to

instrumental mass fractionation, but their behaviour clearly deviates from one another below that NAI threshold.

Instrumental boron isotope mass fractionation II: Release and Diffusion Model (RDM)

In the previous section we reported our experimental observation of strong and systematic impacts of plasma condition on the measured boron isotope ratio i.e., the instrumental mass fractionation. To conceptualise the observations, we consider the processes that occur within the plasma:

(1) laser aerosol is injected into the plasma
(2) aerosol is evaporated and atoms are released
(3) atoms are ionised
(4) ions are sampled from the plasma.

Points 2 and 3 depend on the plasma condition (i.e., temperature or energy density, quantified by the NAI metric), which we link to the degree of sample decomposition. The hotter the plasma, the faster the evaporation, atomisation and ionisation of the material introduced. For colder plasma conditions this can result in differing degrees of incomplete sample decomposition. Additionally, sample atoms and ions released from the aerosol particles undergo collisions with the atoms and ions of the plasma environment. The later likely results in a radial diffusion from the centre trajectory of the initial particle injection. Since both B isotopes differ significantly in their respective masses, the lighter ^{10}B is affected more strongly by this diffusion compared with the about 10% heavier ^{11}B. For a gradual release of boron with increasing plasma temperature (or while the aerosol travels along the temperature gradient within the plasma) the preferential radial diffusion of ^{10}B results in a relative enrichment of ^{11}B in the centre axis of the plasma, which results in a mass fractionation towards heavier ^{11}B/^{10}B ratios for ions sampled.

We simulate this behaviour using a release and diffusion model (RDM). The RDM differs from concepts like space charge effects (e.g., Tanner 1992, Niu and Houk 1996), because it considers processes within the plasma, before the ions are sampled through the cone. It is based on the idea of gradual release of atoms/ions from the injected particles of the laser aerosol, which afterwards are diffusing into the surrounding plasma. On the contrary, space charge effects refer to the repulsion of ions by Coulomb force after the ions have passed the cone, and following separation of electrons from the positively charged ions.

A detailed description of the model is provided in the supplements. In principle the model is based on a predefined gradual release of B along the centre axis of the modelled plasma volume. After release, both ^{10}B and ^{11}B, undergo diffusion which is considered mass-dependent, i.e., ^{10}B is diffusing $\sim$ 10% stronger than ^{11}B. The resulting B intensities and isotope ratios are normalised to their respective maximum. To meet the experimental data only one parameter is adjusted, a common scaling factor for the diffusion parameters of both ^{10}B and ^{11}B. The criterion used for this parameter adjustment is the experimentally estimated B instrumental fractionation of $\sim$ -35‰ at peak B signal intensity (see supporting information).

The results of a typical model run can be seen in Figure 7. The balance between B release and diffusion results in peak B intensity when $\sim$ 77% of total B amount released. The model requires $\sim$ 97% of total B to be released, to result in a fractionation of $\sim$ -17.5‰, the threshold for diminishing matrix-dependent offsets (see previous section). This estimate is not changing significantly when modifying the B release function (Figure S9).

We conclude that to achieve negligible differences in instrumental mass fractionation due to matrix-dependent offsets in B isotopes, almost complete B release ($\sim$ 97%) needs to be accomplished. Plasma conditions that only allow for a lower partial B release, despite resulting in a higher signal intensity, are not robust to changes in the sample matrix. For example, at peak B signal intensity, a 1% difference in B release corresponds to a 0.44‰ change in B isotope instrumental mass fractionation according to the model. Applying this to the trends we observe experimentally (Figure 5), results in B release estimates for the three RMs equal to 77% (epo-951), 83% (NIST SRM 610) and 70% (JCp-1) when we tune for maximum B signal using epo-951. It may seem counter-intuitive that partial B release instead of total, corresponds to maximum signal intensity. According to our model, it is the balance between release and diffusion that controls the signal intensity. The combination for maximum intensity is achieved, when enough B has been released from the laser aerosol particles, but only a small amount has been lost to diffusion. At some point the diffusive loss exceeds the release of B and the signal intensity declines, although additional experiments are needed for a more detailed overview on the B release characteristics specific to different materials.

Another factor that could affect the degree of B release is the mass load. Considering the energy consumed by the processes of sample aerosol evaporation, atomisation and ionisation, increasing mass loads should lower the degree of B release at the position where ions are sampled. Lower B release would, according to our RDM perspective, shift the measured B isotopes towards lighter values. This agrees with observations by for example Kimura et al. (2016) and Sadekov et al. (2019), who show a shift towards lighter B isotope ratios with increasing mass load.

Another finding reported by Kimura et al. (2016) can be contextualised using our model. They reported a gradual shift towards lighter B isotope ratios when measuring off-axis in the plasma. The reported quasi-parabolic decline in measured B isotope ratios by up to -50‰ agrees well with the RDM prediction (see Figure 7).

Conclusions

Two major unrelated issues appear to be responsible for most of the inaccuracies observed in B isotope LA-MC-ICP-MS determinations:

(1) the variable impact on the spectral baselines from both scattered Ar and Ca ions and
(2) variable matrix and mass load dependent degrees of B release from the sample aerosol and the resulting isotope fractionation within the plasma.

The issues with spectral baselines have been reported before. We demonstrate that the baseline problem is present for different types of MC-ICP-MS and that it is clearly correlated to the ion beam intensities of both Ar and Ca ions when boron isotopes are measured using Faraday cups. The baseline can be practically eliminated when deflectors are used to guide the B ion beams, a possibility for all three types of MC-ICP-MS when using ion counters. If the latter is impractical, the baseline signal needs to be monitored and corrected for respective changes. This can be done following offset-correction protocols (Sadekov et al. 2019, Standish et al. 2019, Evans et al. 2021) or directly, by monitoring and correcting for the baseline responses of both Faraday cups used to measure boron isotopes via additional detectors. The recent implementation of collision/reaction cells in latest generation MC-ICP-MS instruments promises a great reduction of the problem. However, if those cells can effectively remove both, Ar and Ca ions, simultaneously, remains to be seen.

The second issue is of more fundamental nature since it affects all types of ICP-MS. The gradual release of boron within the plasma and mass-dependent diffusion seems to have a major impact on the instrumental mass

fractionation. We propose a release and diffusion model (RDM) that can reproduce experimental observations. This model provides an estimate of the minimal degree of B released from the sample aerosol to ensure matrix- and mass-load-independent measurements. Our estimate of ~ 97% highlights the necessity of close to complete B release for fully unbiased B isotope LA-MC-ICP-MS analyses. This high degree of B release can be achieved by opting for hotter plasma conditions (NAI > 4–5). It sacrifices sensitivity (at least by a factor of 2–3), but allows for accurate results. If, however, the application does not allow for any loss in sensitivity the best approach might be more laborious.

First, relative differences between samples can be determined accurately and precisely at high sensitivity (low NAI) plasma conditions, under the condition that only sample material of similar matrix is targeted and analysed under identical analytical conditions (i.e., constant mass load). An example is the application of B isotope mapping, where the sample itself is perhaps the best matrix-matched reference material. Secondly, robust analyses (hot plasma, higher NAI) can be used to calibrate the data measuring representative samples and reference materials. This approach was used recently for B isotope 2D mapping (Fietzke and Wall 2022).

Finally, we want to state clearly, that maxima in sensitivity and accuracy are not achievable for this application at the same time. They clearly are conflicting optimisation goals.

Although, $\delta^{11}B$ carbonate data produced by Sadekov et al. (2019), Standish et al. (2019) and Evans et al. (2021) apply a baseline correction method based primarily on the B/Ca ratio of a particular carbonate sample measured, this approach does not account for both baseline and matrix problems. Such baseline correction schemes might fail if sample material and reference materials are not matched tightly with respect to both matrix and mass load. Furthermore, the RDM developed for this application could become a valuable tool for more general studies into the behaviour of a variety of elements in different sample matrices.

Acknowledgements

Data availability statement

All data used in this study will be provided upon reasonable request.

References

Aggarwal J.K., Sheppard D., Mezger K. and Pernicka E. (2003)
Precise and accurate determination of boron isotope ratios by multiple collector ICP-MS: Origin of boron in the Ngawha geothermal system, New Zealand. Chemical Geology, 199, 331–342.

Aggarwal J.K., Böhm F., Foster G., Halas S., Hönisch B., Jiang S.Y., Kosler J., Liba A., Rodushkin I., Sheehan T., Shen J.J.S., Tonarini S., Xie Q.L., You C.F., Zhao Z.Q. and Zuleger E. (2009)
How well do non-traditional stable isotope results compare between different laboratories: Results from the interlaboratory comparison of boron isotope measurements. Journal of Analytical Atomic Spectrometry, 24, 825–831.

Babila T.L., Penman D.E., Standish C.D., Doubrawa M., Bralower T.J., Robinson M.M., Self-Trail J.M., Speijer R.P., Stassen P., Foster G.L. and Zachos J.C. (2022)
Surface ocean warming and acidification driven by rapid carbon release precedes Paleocene-Eocene Thermal Maximum. Science Advances, 8, 1–13.

Catanzaro E.J., Champion C.E., Garner E.L, Marinenko G., Sappenfield K.M. and Shields W.R. (1970)
Standard reference materials: Boric acid, isotopic, and assay standard reference materials. National Bureau of Standards Special Publication, 260-17, 58pp.

Chalk T.B., Standish C.D., D'Angelo C., Castillo K.D., Milton J.A. and Foster G.L. (2021)
Mapping coral calcification strategies from in situ boron isotope and trace element measurements of the tropical coral Siderastrea sidereal. Scientific Reports, 11, 1–13.

Chaussidon M., Robert F., Mangin D., Hanon P. and Rose E.F. (1997)
Analytical procedures for the measurement of boron isotope compositions by ion microprobe in meteorites and mantle rocks. Geostandards Newsletter: The Journal of Geostandards and Geoanalysis, 21, 7–17.

Evans D., Gerdes A., Coenen D., Marschall H.R. and Müller W. (2021)
Accurate correction for the matrix interference on laser ablation MC-ICP-MS boron isotope measurements in $CaCO_3$ and silicate matrices. Journal of Analytical Atomic Spectrometry, 36, 1607–1617.

references

Fietzke J., Heinemann A., Taubner I., Böhm F., Erez J. and Eisenhauer A. (2010)
Boron isotope ratio determination in carbonates via LA-MC-ICP-MS using soda-lime glass standards as reference material. Journal of Analytical Atomic Spectrometry, 25, 1953–1957.

Fietzke J., Ragazzola F., Halfar J., Dietze H., Foster L.C., Hansteen T.H., Eisenhauer A. and Steneck R.S. (2015)
Century-scale trends and seasonality in pH and temperature for shallow zones of the Bering Sea. Proceedings of the National Academy of Sciences of the United States of America, 112, 2960–2965.

Fietzke J. and Frische M. (2016)
Experimental evaluation of elemental behavior during LA-ICP-MS: Influences of plasma conditions and limits of plasma robustness. Journal of Analytical Atomic Spectrometry, 31, 234–244.

Fietzke J. and Wall M. (2022)
Distinct fine-scale variations in calcification control revealed by high-resolution 2D boron laser images in the cold-water coral Lophelia pertusa. Science Advances, 8, 1–9.

Foster G.L., Ni Y.Y., Haley B. and Elliott T. (2006)
Accurate and precise isotopic measurement of sub-nanogram sized samples of foraminiferal hosted boron by total evaporation NTIMS. Chemical Geology, 230, 161–174.

Foster G.L. (2008)
Seawater pH, p_{CO2} and $[CO_3^{2-}]$ variations in the Caribbean Sea over the last 130 kyr: A boron isotope and B/Ca study of planktic foraminifera. Earth and Planetary Science Letters, 271, 254–266.

Foster G.L., Marschall H.R. and Palmer M.R. (2018)
Boron isotope analysis of geological materials. In: Marschall H.R. and Foster G.L (eds), Boron isotopes: The fifth element. Advances in Isotope Geochemistry (Springer book series), 13–32.

Gonfiantini R., Tonarini S., Groning M., Adorni-Braccesi A., Al-Ammar A.S., Astner M., Bachler S., Barnes R.M., Bassett R.L., Cocherie A., Deyhle A., Dini A., Ferrara G., Gaillardet J., Grimm J., Guerrot C., Krahenbuhl U., Layne G., Lemarchand D., Meixner A., Northington D.J., Pennisi M., Reitznerova E., Rodushkin I., Sugiura N., Surberg R., Tonn S., Wiedenbeck M., Wunderli S., Xiao Y.K. and Zack T. (2003)
Intercomparison of boron isotope and concentration measurements. Part II: Evaluation of results. Geostandards Newsletter: The Journal of Geostandards and Geoanalysis, 27, 41– 57.

Gutjahr M., Bordier L., Douville E., Farmer J., Foster G.L., Hathorne E.C., Hönisch B., Lemarchand D., Louvat P., McCulloch M., Noireaux J., Pallavicini N., Rae J.W.B., Rodushkin I., Roux P., Stewart J.A., Thil F. and You C.-F. (2021)
Sub-permil interlaboratory consistency for solution-based boron isotope analyses on marine carbonates. Geostandards and Geoanalytical Research, 45, 59–75.

Hathorne E.C., Gagnon A., Felis T., Adkins J., Asami R., Boer W., Caillon N., Case D., Cobb K.M., Douville E., de Menocal P., Eisenhauer A., Garbe-Schönberg D., Geibert W., Goldstein S., Inoue M., Kawahata H., Kölling M., Cornec F.L., Linsley B.K., McGregor H.V., Montagna P., Nurhati I.S., Quinn T.M., Raddatz J., Rebaubier H., Robinson L., Sadekov A., Sherrell R., Sinclair D., Tudhope A.W., Wei G., Wong H., Wu H.C. and You C.F. (2013)
Interlaboratory study for coral Sr/Ca and other element/Ca ratio measurements. Geochemistry Geophysics Geosystems, 14, 3730–3750.

Hemming N.G. and Hanson G.N. (1992)
Boron isotopic composition and concentration in modern marine carbonates. Geochimica et Cosmochimica Acta, 56, 537–543.

Jochum K.P., Weis U., Stoll B., Kuzmin D., Yang Q., Raczek I., Jacob D.E., Stracke A., Birbaum K., Frick D.A., Günther D. and Enzweiler J. (2011)
Determination of reference values for NIST SRM 610–617 glasses following ISO guidelines. Geostandards and Geoanalytical Research, 35, 397–429.

Kimura J.I., Chang Q., Ishikawa T. and Tsujimori T. (2016)
Influence of laser parameters on isotope fractionation and optimisation of lithium and boron isotope ratio measurements using laser ablation multiple Faraday collector-inductively coupled plasma-mass spectrometry. Journal of Analytical Atomic Spectrometry, 31, 2305–2320.

Lecuyer C., Grandjean P., Reynaud B. Albarède F. and Télouk P. (2002)
$^{11}B/^{10}B$ analysis of geological materials by ICP-MS Plasma 54: Application to the fractionation between brachiopod calcite and seawater. Chemical Geology, 186, 45–55.

Le Roux P., Shirey S.B., Benton L., Hauri E.H. and Mock T.D. (2004)
In situ, multiple-multiplier, laser ablation ICP-MS measurement of boron isotopic composition ($\delta^{11}B$) at the nanogram level. Chemical Geology, 203, 123–138.

Marschall H.R. and Foster G.L. (eds.) (2018)
Boron isotopes: The fifth element. Advances in Isotope Geochemistry (Springer book series), 351pp.

May W.E. and Gills T.E. (1999)
Standard reference material 951 boric acid standard. National Institute of Standards and Technology Certificate of Analysis, 1–2.

Mayk D., Fietzke J., Anagnostou E. and Paytan A. (2020)
LA-MC-ICP-MS study of boron isotopes in individual planktonic foraminifera: A novel approach to obtain seasonal variability patterns. Chemical Geology, 531, 1–9.

references

McMullen C.C., Cragg C.B. and Thode H.G. (1961)
Absolute ratio of $^{11}B/^{10}B$ in Searles Lake borax.
Geochimica et Cosmochimica Acta 23, 147–150.

Niu H. and Houk R.S. (1996)
Fundamental aspects of ion extraction in inductively coupled plasma-mass spectrometry. **Spectrochimica Acta Part B**, 51, 779–815.

Palmer M.R. and Swihart G.H. (1996)
Boron isotope geochemistry: An overview. In: Grew E.S. and Anovitz L.M. (eds), Boron: Mineralogy, petrology, and geochemistry (Volume 33). Mineralogical Society of America (Chantilly), 709–740.

Raitzsch M., Rollion-Bard C., Horn I., Steinhöfel G., Benthien A., Richter K.U., Buisson M., Louvat P. and Bijma J. (2020)
Single-shell δ^{11}B analysis of *Cibicidoides wuellerstorfi* using femtosecond laser ablation MC-ICP-MS and secondary ion mass spectrometry. **Biogeosciences**, 17, 5365–5385.

Sadekov A., Lloyd N.S., Misra S., Trotter J., D'Olivo J. and McCulloch M. (2019)
Accurate and precise microscale measurements of boron isotope ratios in calcium carbonates using laser ablation multicollector-ICP-MS. **Journal of Analytical Atomic Spectrometry**, 34, 550–560.

Spivack A.J. and Edmond J.M. (1986)
Determination of boron isotope ratios by thermal ionization mass spectrometry of the dicesium metaborate cation. **Analytical Chemistry**, 58, 31–35.

Standish C.D., Chalk T.B., Babila T.L., Milton J.A., Palmer M.R. and Foster G.L. (2019)
The effect of matrix interferences on *in situ* boron isotope analysis by laser ablation multi-collector inductively coupled plasma-mass spectrometry. **Rapid Communications in Mass Spectrometry**, 33, 959–968.

Tanner S.D. (1992)
Space charge in ICP-MS: Calculation and implications. **Spectrochimica Acta Part B**, 47, 809–823.

Wall M., Fietzke J., Crook E.D. and Paytan A. (2019)
Using B isotopes and B/Ca in corals from low saturation springs to constrain calcification mechanisms. **Nature Communications**, 10, 3580.

Supporting information

The following supporting information may be found in the online version of this article:

Appendix S1. Preparation of epo-951 reference material.

Appendix S2. Chemical characterisation of boric acid epoxy pellet epo-951.

Appendix S3. Overview of possible contributions to inaccuracies in B isotope LA-MC-ICP-MS measurement.

Appendix S4. Additional information regarding test data.

Appendix S5. Release and diffusion model (RDM).

Table S1. Operating parameters for the different MC-ICP-MS types used in this study.

Figure S1. Mind map: Components and likely effects involved in LA-MC-ICP-MS analysis of boron isotopes.

Figure S2. Spectral baseline scans measured on IC6 under different plasma conditions (a) 1200 W rf test series, (b) 1000 W rf test series.

Figure S3. Correlation between baseline intensity measured at 10.505 amu (IC6 spectral position during B isotope Faraday cup multi-collection) and IC6 baseline peak intensity at 10.54 amu.

Figure S4. Changes in relative signal intensity of ^{11}B and ^{43}Ca and the relative sensitivity ratio ^{11}B/^{43}Ca depending on plasma condition (NAI).

Figure S5. Examples of background signal intensities mass scans around 10 amu for (a) AXIOM, (b) Neptune plus and (c) Nu Plasma3 using Faraday cups or ion counters.

Figure S6. Example of a release function used in the model runs, a Gaussian centred at $Z = 200$ and σ of 30.

Figure S7. Calculation scheme for the step from layer Z to $Z+1$ to simulate the mass-dependent diffusion of ^{10}B and ^{11}B.

Figure S8. Trend of relative boron isotope fractionation *vs.* NAI.

Figure S9. Release and diffusion model (RDM) results using three different release functions, all centred at $Z = 200$, but with σ equal to 50 (left), 30 (middle) and 10 (right panels).

Figure S10. Trends of boron isotope fractionation *vs.* B release for the three RDM runs displayed in Figure S8.

This material is available from: http://onlinelibrary.wiley.com/doi/10.1111/ggr.12511/abstract (This link will take you to the article abstract).